3D CSEM inversion strategy: an example offshore west of Greenland

A. Lovatini, M.D Watts,.K. Umbach, A. Ferster
WesternGeco EM – Geosystem, Milan, Italy
EnCana Corporation, Calgary, Canada

Copyright 2009, SBGf - Sociedade Brasileira de Geofísica

This paper was prepared for presentation during the 11th International Congress of the Brazilian Geophysical Society held in Salvador, Brazil, August 24-28, 2009.

Contents of this paper were reviewed by the Technical Committee of the 11th International Congress of the Brazilian Geophysical Society and do not necessarily represent any position of the SBGf, its officers or members. Electronic reproduction or storage of any part of this paper for commercial purposes without the written consent of the Brazilian Geophysical Society is prohibited.

Abstract

Although there have been many publications on theoretical aspects of marine CSEM, covering most elements from data processing through to inversion, there have been few on interpretation and practical use of these data. Amongst these, significant contributions have been made by: Carazzone et al. for subsalt exploration in Brazil (2008) and in Angola (2005), Buonora et al. (2008) in Brazil, Price et al. (2008) in Nigeria, and Darnet et al. (2007) in Malaysia. In this paper, we show how multidimensional inversion and interpretation contribute to the ranking of prospects in two blocks west of Greenland. In both, the geological targets are Cretaceous sandstones in elongate structures; known complicating factors include the presence of shallow resistive volcanics and the intermittent presence of crystalline basement at relatively shallow depths below some of the targets.

Introduction

In the summer of 2008, after a detailed survey design, WesternGeco Electromagnetics carried out a large survey offshore west of Greenland for the EnCana Corporation acquiring CSEM, MT, gravity and magnetic data. The survey covered two different blocks for a total of more than 1000 km of tow lines and more than 200 EM receivers (Figure 1). On completion of the acquisition phase, WesternGeco EM worked in close cooperation with Encana to produce an integrated CSEM and MMT interpretation workflow to increase the confidence in the geological model of the two areas and rank the possible prospects.

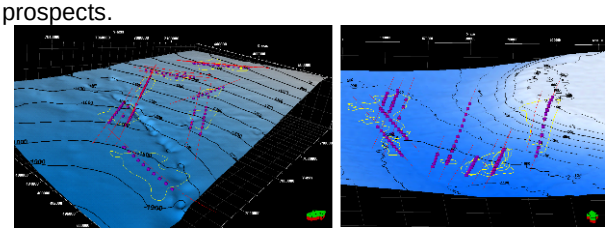

Figure 1; Survey area bathymetry and CSEM tow line and receiver design for the two blocks

Survey design

Before the survey, extensive use was made of all a priori information (seismic horizons and well logs) to assess the sensitivity of the CSEM method for the expected targets in order to optimize the survey design in terms of transmitter and receiver layout and acquisition parameters.

The first step consisted of building preliminary 1D scenarios and using the synthetic model responses to verify the sensitivity by means of a normalized amplitude/phase difference approach over a wide range of frequencies. The analysis was extended to 3D modeling only for target that proved 1D sensitivity, i.e., the ones with anomalous responses that exceeded a 20% variation and were clearly above the system noise threshold (conservatively set to 10-15V/Am2 for the electric field measurements).

3D modeling is essential in survey design (Bornatici et al., 2007) to properly evaluate the target responses: 1D modeling where any layer has an infinite extension in both X and Y directions grossly overestimates possible responses and fails to take into consideration variably bathymetry and geology.

Geosystem's finite-difference code was used for 3D modeling and inversion (Mackie et al. 2007; Rodi and Mackie 2001). The resistivity volumes were built using the seismic horizons as resistivity boundaries and resistivity values were chosen from neighboring (less than 200 km away) well logs (Figure 2). For each investigated prospect, with- and without-target scenarios were computed to generate synthetic CSEM responses. Normalized amplitude and phase difference sensitivity maps and pseudosections were utilized to revise the 1D modeling detectability to define the optimal frequency/offset combination for each prospect area.

In designing the receiver and tow line positions, the above considerations were used as guidelines together with bathymetric considerations to optimize the cost/benefit ratio of the survey. The waveform was designed to maximize the energy at the frequency that showed the best trade-off between earth penetration and target response magnitude. At the high latitude of the survey, strong magnetotelluric signal (due to proximity to the polar electro jet) was expected, and because it could significantly affect the CSEM signal, the waveform base period was selected to give the best signal-to-noise ratio (SNR).

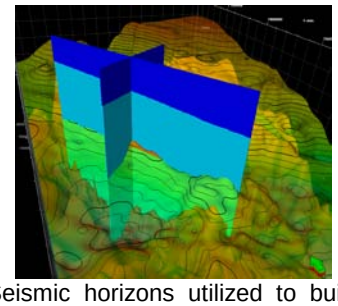

Figure 2; Seismic horizons utilized to build the three-dimensional resistivity models, the with target scenario model is shown here in two perpendicular sections.

On-board processing and data QC

The data continuously recorded at the receiver locations are processed together with the transmitter current time series and the stream of navigation data describing the dipole instantaneous geometry and positions along the tow line. The three different streams are synchronized and subsequently segmented to be merged and transformed in frequency domain. The processing stage is critical to produce reliable data to be used in the interpretation workflow. QC and processing flow software was used (Figure 3 and Figure 4) that was capable of processing three-dimensional receiver spreads and several tow lines while considering the instantaneous variations in both the data and acquisition geometry and estimating the instantaneous noise component associated. The introduction of the SNR estimation allowed discrimination of usable and non-usable data and assignment of a SNR-driven confidence value to each data sample. Displays such as normalized pseudosections and common offset maps were used for QC purposes; as interpretational devices they were seriously misleading due to the influence of shallow irregular volcanic resistors.

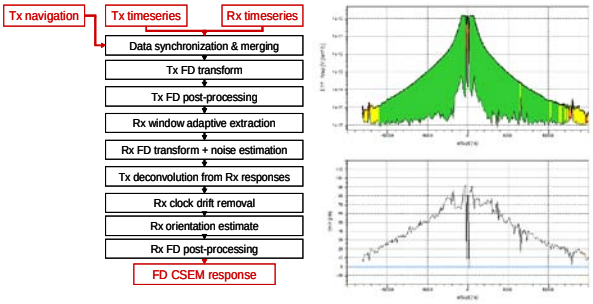

Figure 3; On the left, WGEM CSEMXpress processing workflow. On the right, amplitude versus offset plot colour coded by the signal-to-noise ratio (above) and SNR versus offset plot (below).

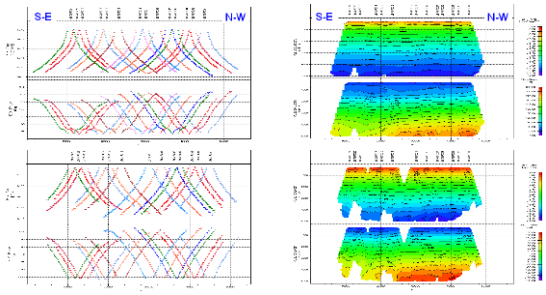

Figure 4; WGEM CSEMXpress standard on-board QC products. On the left, E and H tow line MVO/PVO gather. Oon the right, E and H amplitude and phase pseudosections.

Integrated interpretation: The method

1D inversions are theoretically limited in terms of geology sensitivity to quasi-infinitely extended targets, but in reality, they have two main advantages: the benefit of accurately recovering the background resistivity distribution and a sharp sensitivity to shallow targets. The background resistivity distribution matched quite accurately the resistivity distribution determined from distant (150 km) wells. apart from a multiplicative factor around 2 that is explained by the primary sensitivity of inline CSEM data to the vertical component of resistivity rather than the horizontal resistivity measured by most logging tools. Broadside data 1D inversions including anisotropy confirmed this factor between vertical and horizontal resistivity.
The resistivity distribution derived from well logs and revised with the 1D inversions, together with horizons from seismic interpretation, were used to build the 3D resistivity models used as the starting point for inversion. Our 3D inversion code allows exploiting fully the tridimensional nature of both source and geology, including the possible anisotropic distribution of each resistivity cell in the unknowns.

Integrated interpretation: synthetic and observed data examples

In the example below, we demonstrate that the inversion technique correctly recovers the starting model from synthetic data, and that artifacts, in particular, potentially interesting resistors, are not introduced. We also verify that the 3D inversion sensitivity to the expected target.
Synthetic 3D responses using the actual survey acquisition parameters (frequencies), coverage (inline and broadside), and instantaneous source geometry were generated using forward modeling from two different 3D models. In one case, the target was included; in the other, it was not inserted in the model. Both synthetic datasets were 3D inverted, and in both cases, the inversion succeeded in reconstructing a model close to the a priori one. In a third test, the most critical, the synthetic dataset with target included was inverted starting from a model close to the area geology excluding the target. The inversion result was positive and showed that a resistivity feature was needed to fit the data, depth, and lateral

extensions of this feature, matching the ones of target included in the model that originated the data (Figure 5).
The same inversion settings and a priori model were then used to invert the observed data (Figure 6). The resulting resistivity volume confirmed shallower, slightly resistive features as indicated by 1D inversions, but inserted a resistivity feature in the model (> 10 Ohm.m) that conformed to the expected depth and lateral extent of the target. The synthetic responses obtained from the inversion model fit the observed data well for both the inline and broadside cases (Figure 7). This result, together with the target shape, adds credibility to both the geophysical and geological validity of the inversion output.

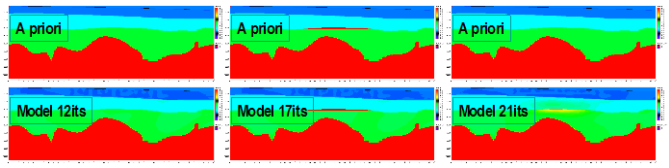

Figure 5; Synthetic data study: from the left, the a priori model and 3D inversion resistivity output of three different tests are show;., In the first two examples, the synthetic data used in the inversion were generated from the same model used as a prior;, in the third, the synthetic data were generated by the second example a priori model.

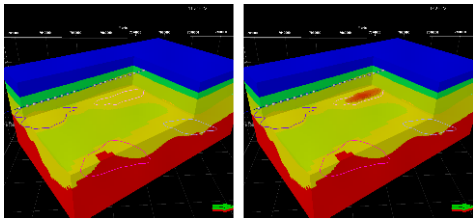

Figure 6; On the left, resistivity volume used as a priori model in the inversion of observed data; on the right, same model plus superimposed the inversion output model resistivities above 10 Ohm.m

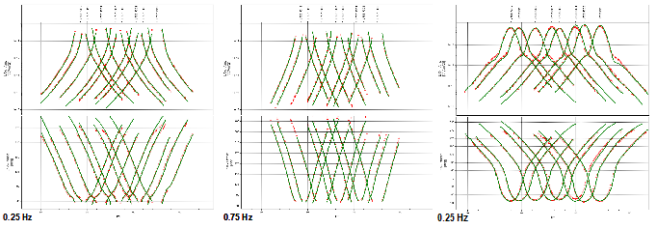

Figure 7; Data misfit between observed data (red dots) and 3D inversion calculated data (green line). On the left, inline data at two different frequencies; on the right, broadside illumination case

Conclusions

The workflow we presented was applied in the west of Greenland survey for all the leads on the two blocks to give an image for each one that allowed them to be ranked. The CSEM method gave complementary information on the resistivity properties, which, closely integrated with seismic and geological knowledge, contributed to the evaluation of these targets.

References

Abma, R., Sun, J. , & Bernitsas, N., 1999, Antialiasing methods in Kirchhoff migration: Geophysics, 64. 1783-1792

Bornatici, L., Mackie, R., and Watts, M.D., 2007, 3D inversion of marine CSEM data and its application to survey design. EGM 2007 conference proceedings.

Buonora, M.P., Zerilli, A., Labruzzo, T., and Rodrigues, L.F., 2008, Advancing marine controlled source electromagnetics in the Santos basin, Brazil. 70th EAGE Conference & Exhibition, Extended Abstracts.

Carazzone, J.J, Dickens, T.A., Green, K.E., Jing, C., Wahrmund, L.A., Willen, D.E., Commer, M., and Newman, G.A., 2008, Inversion study of a large marine CSEM survey. 78th Annual International Meeting, SEG, Expanded Abstracts, 27, 644

Carazzone, J.J., Burtz, O.M., Green, K.E., Pavlov, D.A., and Xia, C., 2005, Three Dimensional Imaging of Marine CSEM Data. 75th Annual International Meeting, SEG, Expanded Abstracts, 24, 575

Darnet, M., Choo, M.C.K., Plessix, R.E., Rosenquist, M.L., Yip-Cheong, K., Sims, E., and Voon, J.W.K., 2007, Detecting hydrocarbon reservoirs from CSEM data in complex settings: Application to deepwater Sabah, Malaysia. Geophysics, 72, WA97

Mackie, R., Watts, M.D., Rodi, W., 2007, Joint 3D inversion of marine CSEM and MT data. 77th Annual International Meeting, SEG, Expanded Abstracts, 26, 574.

Price, A., Turpin, P., Erbetta, M., Watts, M.D., and Cairns., G., 2008, 1D, 2D and 3D modeling and inversion of 3D CSEM data offshore West Africa. 78th Annual International Meeting, SEG, Expanded Abstracts 27, 639
Rodi, W.L., and Mackie, R.L., [2001] Nonlinear conjugate gradients algorithm for 2-D magnetotelluric inversion. Geophysics, 66, 174-187.